AUTOMATIC RECONSTRUCTION OF BRAIN'S MICRO-VASCULAR NETWORK BASED ON X-RAY SYNCHROTRON TOMOGRAPHY

Kristóf Kapitány[1], László Négyessy[2,3], Caroline Fonta[4], Rajmund Mokso[5], Zsuzsanna Szepessy[6], Árpád Barsi[1]

[1] Department of Photogrammetry and Geoinformatics, Budapest University of Technology and Economics
[2] Wigner Research Centre for Physics, Hungarian Academy of Science
[3] Department of Anatomy, Histology and Embryology, Semmelweis University
[4] Centre de Recherche Cerveau et Cognition, Université P Sabatier
[5] Swiss Light Source, Paul Scherrer Institut
[6] Department of Ophthalmology, Semmelweis University

kapitany.kristof@epito.bme.hu

Abstract

X-ray synchrotron tomographic microscopy enables the acquisition of large amount of images with a geometric and radiometric resolution sufficient for the morphometric and topologic analysis of vascular and even of microvascular network of different organs. In this study cylindrical shaped, NiDAB labelled brain samples of a diameter of half a millimeter were imaged and analyzed with an effective pixel size of $0.38\,\mu$m. Several thousands of tomographic slices build up each reconstructed volume meaning that an automatized analysis tool is indispensable. These big data sets are processed by the developed algorithms on commercially available PCs with an automated image analysis technology in acceptable processing time. The obtained vessel segments are stored for further topological and morphometric analyses or surface/volumetric visualization purposes. These analyses contain vessel feature distribution analysis followed by 3D reconstruction. The obtained results are in accordance to the literature data.

Keywords: image processing, object reconstruction, 3D modelling, micro punching, high throughput, vascular network, cerebral cortex

1. Introduction

The knowledge of brain blood circulation is essential to understand the functioning and diseases of the brain. The imaging techniques of nowadays is getting more important thanks to the increasing quality, resolution and speed of image acquisition. Our research focuses on the algorithmic development to process these imagery, especially on handling large amount of images. A very promising imaging technique is the X-ray synchrotron tomography (XRST), where the synchrotron delivers bright photon beam with the possibility to selectively tune the wavelength to fulfill the requirements imposed by the sample size and its electron density. In addition to the attenuation we can also exploit the refraction of the X-ray wave-front on the interfaces in the sample arising as a consequence of the partial coherence of synchrotron X-ray beams[1] This unique combination of attenuation and phase contrast is very useful for the studies of the vascular system at the micrometer scale. The spatial resolution in the three dimensional volumetric representation of the sample is isotropic and is determined

by the pixel size of the detector, the numerical aperture of the objective and the phosphor screen thickness converting the X-rays to visible light.[2]

From the large XRST data sets of micrometer resolution, it is reliable to characterize morphometric and topological characteristics of vessels networks.[3-5] Moreover such data provide vessel networks that can be used as a realistic basis for a numerical simulation of hemodynamic phenomena inside tens of cubic millimeters of cerebral cortex, which at the present time are not accessible through experimental measurements. XRST is applicable post mortem, which is very important in human studies. Also, XRST does not require complicated histological processing for vessel visualization.

The developed complete 3D model is suitable for morphometric analysis of vascular network of brain tissues. For the reconstruction we developed software in Matlab environment.

Materials

XRST images were obtained from different samples of cerebral cortex of an adult marmoset (*Callithrix jacchus*). The animal was treated in accordance with the Guide for the Care and Use of Laboratory Animals (National Research Council 1996), European Directive 86/609 and the guidelines of the local institutional animal care and use committee.

Transcardial perfusion of an aldehyde solution was applied to preserve brain structure and the samples were treated with Avidin Biotin Complex (ABC) protocol (Elite kit, Vector Laboratoires, Burlingame, CA 94010, USA) and nickel-intensified diaminobenzidine (Ni-DAB; Sigma-Aldrich, Saint-Quentin Fallavier, France) as the chromogen.[6] After the NiDAB reaction, sample A9 was osmicated (1% OsO_4, Electron Microscopy Sciences, Hatfield, PA

19440, USA) and 5% sucrose in PB for 60 minutes). All three samples were dehydrated and infiltrated with resin as described above. In order to contrast x-ray-imaged vessels, barium sulfate solution was perfused in the general blood circulation in advance of the transcardial perfusion, according to the protocol described in Plouraboué et al. (2004) and Risser et al. (2009).[7,4]

Method

The samples were imaged at the TOMCAT beamline[2] of the Swiss Light Source at the Paul Scherrer Institut in Switzerland using XRST. Monochromatic synchrotron X-rays were used for the probing radiation with an energy of 10 keV (wavelength of 0.12 nm). The X-ray beam traversing the sample produces shadow images that were recorded by a CCD camera coupled to a scintillator screen through a microscopic objective with a 20x magnification. The effective pixel size of the detector system was 0.38 μm. The specimens were rotated during acquisition with the axis perpendicular to the X-ray beam direction. With 1501 radiographic projections the angular range of 180° was covered in an equidistant manner to obtain tomographic images. Each sample consists of 2048^3 pixels covering a cylinder with a height and diameter of 780 μm both. According to the stance and position the unnecessary images were removed. *Figure 1* shows a small detail of the tomographic slices.

According to the size of the specimens each examined sample was represented on numerous cross-sections. Because of the high amount data manual image processing is not an option. The presented method could replace this labor-intensive, yet inefficient work by automated algorithms using predefined parameters. The parameters are depending on the sample's shape and size, and on the staining method of the samples. Also the condition of the sample

has to be taken in consideration because the samples could have internal cracks, or the surface of the sample could contain dirt particles or metal fragments and tissue shreds make it in generally rough.

The image processing starts with the segmentation of the vessel cross-sections using predefined intensity values. The vessels has been stained only non-homogenously, therefore it needed additional image enhancement technics, like local rescaled-range calculation (LRRC) that is used generally for texture analysis.[8] This method processes the whole image by dividing it into smaller regions, and evaluating the intensity range inside the neighborhood of each pixel. The implementation of the LRRC technique supports to detect the texture of an image therefore the non-homogenous staining process could be compensated.

After segmentation noise filtering or sample's imperfection removal is necessary. A digital "punch" technique was applied, that cuts off the unwanted part from the detected segments,[9] and contain the analysis of statistics of each region to remove misassignments.

The developed method supports two types of vessel reconstruction solution: a generalized model of the vessels and a surface model of the vessels. Both type requires different input data.

The *generalized model* contains multiple developed visualization and analysis procedures, but the connection must be established between the discrete regions. It has to be determined which regions compose a continuous vessel, and where bifurcations are located. The developed method analyzes and collects statistics about each vessel cross-section. The centroid's coordinates and the matching semi-minor axis lengths of each detected region are used. Each centroid is projected to the adjacent tomographic slices and a search radius is drawn with the length of the matching semi-minor axis around the projections on the particular slices, including one around the centroid itself. Then the number of detected centroids inside the projected circles is counted, and if there is one or more centroids inside, the detected elements are supposedly connecting. Each element is labeled uniquely, but in case of the connection is stated between different centroids, all get the same identification number, therefore continuous vessel branches could be located. At each bifurcation the vessels are partitioned, and the labels of the sub-branches differ, so it is important to recognize the breakpoints. This identification method provides opportunity to analyze both vessel cross-section and the connected elements together.[10]

For the reconstruction of the *surface model* of the vessels, the boundary of each detected ves-
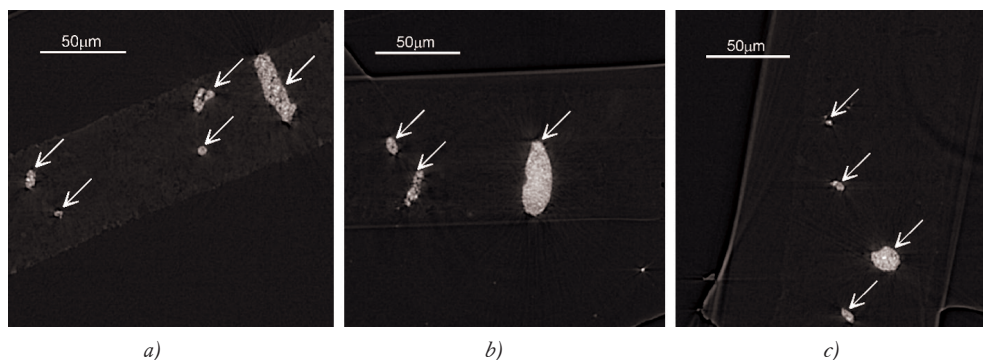

a)   b)   c)

Figure 1. Tomographic slices of Sample A9 *(a)*, Sample A12 *(b)*, Sample A14 *(c)*.
Arrows point to vessel cross-sections

sel cross-section is extracted. The coordinates of each boundary pixel are exported from the images resulting in a large, three-dimensional data set, where a triangulated irregular network (TIN) surface is fitted (*Figure 3*).

Results & Discussion

The developed method has been performed on several samples processed with XRST compatible histological techniques. NiDAB staining resulted in enough parenchymal background staining, which allowed the labeling of the vessels.

Image processing including vessels and branching pattern reconstruction is an automated process. It took 2378 seconds with Matlab on a regular PC for a 1135-slice sample (A9). The image analysis methodology can be taken as of computation requirement of 2.1 sec/image.

Figure 2 presents the detected boundaries of the vessel cross-sections with white outlines, on the same images of *Figure 1*.

Table 1 presents statistics describing the samples and the detected vessel structure. Row no. (3) shows the number of pixels in the direction parallel to the tomographic rotation axis, hence the number of reconstructed to-

mographic slices for the given sample processed. Although the sample's volume maybe similar in the different cases (11), the sample can be represented on a smaller number of tomographic slices depending on the orientation during the tomographic acquisition. The algorithm detects vessel cross-sections (4) on each tomographic slice and connects them together into separate vessel segments (5). At every bifurcation the vessels are partitioned, so the vessel segments are obtained with different identification numbers. The result of vasculature analysis of sample A12 is shown in *Figure 4*. A segment of the tissue was analyzed, and three perpendicular cross-sections containing $200 \times 200 \times 200$ voxels are presented, where the voxel size is $0.38\,\mu\text{m} \times 0.38\,\mu\text{m} \times 0.38\,\mu\text{m}$.

The calculation of statistics was software based and did not require user interaction. Table 1 presents also some derived statistical data about the vascular morphometry in each experimental condition. Vessel segments have the meaning of vessel fragments labeled uniquely (5). The table indicates the mean- (7) and longest length (6) of the identified vessel segments. Median (10), mean and standard deviation (9) of vessels' diameter are also presented. The total length (8) and volume (12) of the reconstructed vessels are used to evaluate the tissue blood supply by calculating the ratio of vascular length to the volume of the tissue

a)   *b)*   *c)*
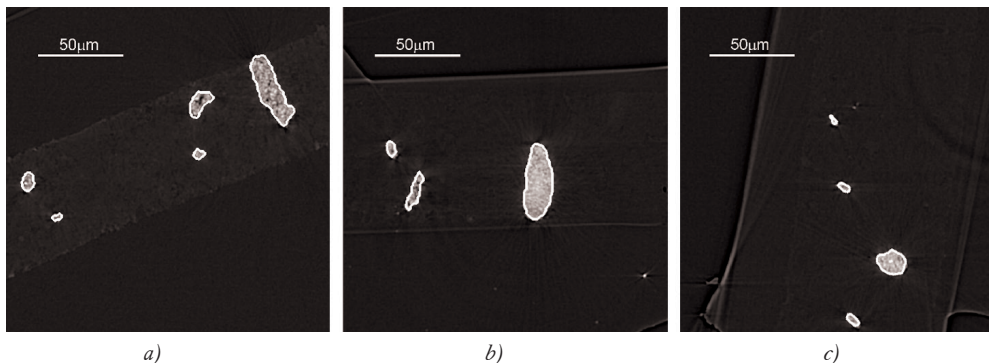
Figure 2. Tomographic slices of Sample A9 *(a)*, Sample A12 *(b)*, Sample A14 *(c)*. White outlines represents vessel cross-sections

Sample's name		A9	A12	A14
1.	Staining method	NiDAB, OsO$_4$, Barium	NiDAB, Barium	NiDAB, Barium
2.	Sample size (cylindrical shape, diameter $\times$ thickness) [μm]	500×60	500×90	300×90
3.	Number of images	1135	915	460
4.	Number of detected vessel cross-sections	6058	8854	2901
5.	Number of detected vessel segments	934	2190	843
6.	Length of the longest vessel [μm]	69.16	49.02	50.16
7.	Mean length of vessel segments [μm]	2.46 ± 5.82	1.54 ± 3.51	1.31 ± 3.81
8.	Full length of detected vessels [μm]	2302.04	3364.52	1102.38
9.	Vessel diameter (mean $\pm$standard deviation) [μm]	3.99 ± 3.14	1.91 ± 2.06	1.43 ± 1.47
10.	Median of the vessels' diameter [μm]	3.37	1.30	1.47
11.	Volume of the examined sample [μm^3]	11 780 972	17 671 458	6 361 725
12.	Total vessel volume [μm^3]	235 060.89	176 375.62	53 672.1
13.	Relative volume of vessels [%]	2.00	1.00	0.84
14.	Tissue supply (vessel length/ tissue volume) [μm/ μm^3]	1.954×10^{-4}	1.904×10^{-4}	1.733×10^{-4}

Table 1. Statistical analysis of the examined samples

sample (14) and the volume of vessels relative to the tissue sample volume (13). Vessel volume is calculated from the number of voxels in each vessel cross-section.

This study describes a high throughput automated process of reconstruction and analyses of brain tissue vasculature at high resolution. The applied XRST technique doesn't require complicated histological processing. The present study also provides evidence for the interest to use micro-tomography in brain research, as it provides large dataset appropriate for automated processing in a reasonable time. XRST
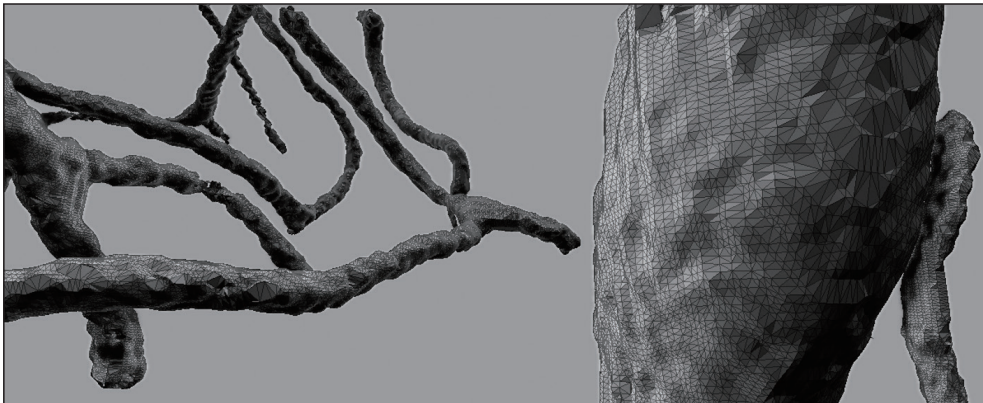

Figure 3. Surface mesh, fitted to the vessel boundaries – a detail of the reconstruction of sample A12

has a great advantage against multiphoton laser microscopy, scanning electron microscopy or optical confocal microscopy, namely this technique has excellent spatial resolution in the range of micrometer level and has not the depth limitation of a few hundreds of micrometers.[7]

Previous studies based on XRST of vessel used barium staining. However, inherent of the process is the uncertainty of complete perfusion especially of the fine vessel branches by the barium staining suspension. This is a major obstacle in studying the finest branches, which are the most vulnerable in clinical conditions.

However, the distribution of the vessels is not homogeneous at a small scale,[3] whose size is close to the thickness of the sample (50-60 μm). Therefore situation may be different from one sample to another, independently of the staining method.

Concerning the morphometry data, our results are similar to those published previously. The vascular length (tissue supply) is comparable, but smaller: 269 mm/mm^3 in marmoset monkeys;[4] our values are between 173 and 195 mm/mm^3. The relative volumes of vessels are also similar to the literature, where 2.5% stands against our finding of 0.84-2%. The longest vessel segment lengths are also very close to the literature: our values are between 49 and 69 μm.[4]

There is a strong evidence that changes in parameters such as vessel diameter, tortuosity and density are related to the disease in large vessels,[11-15] few results are reported at the microscopic scale.[11,16] Therefore it is interesting to develop a multiscale approach and innovative quantitative analysis tools to characterize the capillary networks at different steps of the disease progression in the brain.

Summarizing the benefits of the developed method, we would highlight the following features:
- suitable on commercially available PCs (no need for high performance computers),
- automated image analysis technology (no need for manual work of human operators),
- acceptable processing time (required processing time is ～2 seconds per image).

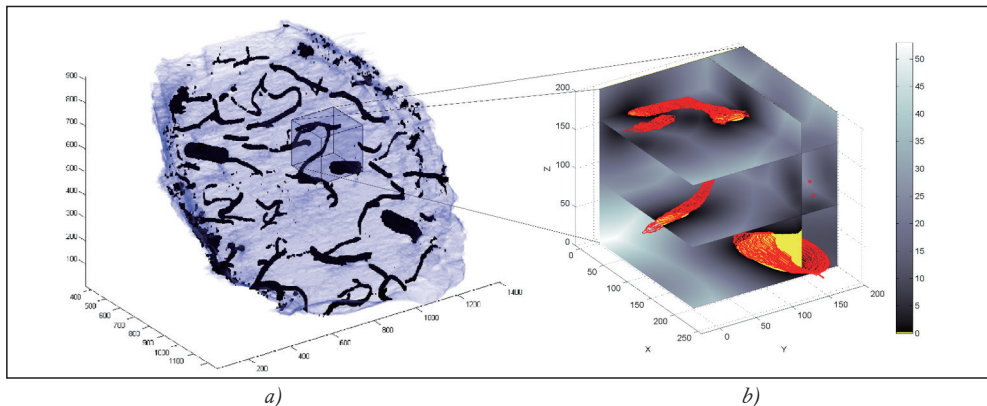*a)*   *b)*

Figure 4. Vascularity analysis. Sample A12 with highlighted vessels (black outlines) *(a)* and an analyzed part in detail *(b)*. The gray scale shows the distance of any point of the tissue from the vessels. The vessels' boundaries are presented in red. This analysis shows that the largest distance between any point of the tissue and the closest vessel is around 50μm. The coordinates and the color bar are in μm (voxel size 0.38 μm × 0.38 μm × 0.38 μm, and 200 × 200 × 200 voxels are represented)

References

1. *Mokso R, Marone F, Irvine S, Nyvlt M, Schwyn D, Mader K, et al.* Advantages of phase retrieval for fast X-ray tomographic microscopy. J Physics D: Appl Phys 2013;46(49):494004, DOI: 10.1088/0022-3727/46/49/494004.

2. *Stampanoni M, Marone F, Modregger P, Pinzer B, Thüring T, Vila-Comamala J, et al.* Tomographic hard X-ray phasecontrast micro- and nano-imaging at Tomcat. AIP Conference Proceedings, 2010;1266:13-7, DOI: 10.1063/1.3478189.

3. *Risser L, Plourabou é F, Steyer A, Cloetens P, Le Duc G, Fonta C.* From homogeneous to fractal normal and tumorous microvascular networks in the brain. Journal of Cerebral Blood Flow and Metabolism 2007;27(2):293-303.

4. *Risser L, Plourabou é F, Cloetens P, Fonta C.* A 3D-investigation shows that angiogenesis in primate cerebral cortex mainly occurs at capillary level. International Journal of Developmental Neuroscience 2009;27(2):185-96, DOI: 10.1016/j.ijdevneu.2008.10.006.

5. *Heinzer S, Krucker T, Stampanoni M, Abela R, Meyer EP, Schuler A, et al.* Hierarchical micro-imaging for multiscale analysis of large vascular networks. Neuroimage 2006;32(2):626-36.

6. *Negyessy L, Gal V, Farkas T, Toldi J.* Cross-modal plasticity of the corticothalamic circuits in rats enucleated on the first postnatal day. Eur J Neurosci 2000;12(5):1654-68.

7. *Plourabou é F, Cloetens P, Fonta C, Steyer A, Lauwers F, et al.* High resolution X-ray imaging of vascular networks. J Microsc 2004;215:139-48.

8. *Russ JC.* Image Processing Handbook. 3rd ed 1998; ISBN: 0-8493-2532-3.

9. *Kapitány, K.* Geometric reduction of high amount histological image data - A digital-punch approach. Conference of Junior Researchers in Civil Engineering; 2012; Budapest; p. 77-82.

10. *Kapitány, K.* Automatic generation and storage of vascular network topology. Second Conference of Junior Researchers in Civil Engineering; 2013; Budapest; p. 1-5.

11. *Meyer EP, Ulmann-Schuler A, Staufenbiel M, Krucker T.* Altered morphology and 3D architecture of brain vasculature in a mouse model for Alzheimer's disease. Proceedings of the National Academy of Sciences of the United States of America 2008;105(9):3587-92.

12. *Dorr A, Sahota B, Chinta LV, Brown ME, Lai AY, et al.* Amyloid-beta-dependent compromise of microvascular structure and function in a model of Alzheimer's disease. Brain 2012;135(Pt 10):3039-50, DOI: 10.1093/brain/aws243.

13. *Biron KE, Dickstein DL, Gopaul R, Jefferies WA.* Amyloid triggers extensive cerebral angiogenesis causing blood brain barrier permeability and hypervascularity in Alzheimer's disease. PLoS One 2011;6(8):e23789

14. *Brown WR, Thore CR.* Review: cerebral microvascular pathology in ageing and neurodegeneration. Neuropathol Appl Neurobiol 2011 Feb; 37(1):56-74, DOI: 10.1111/j.1365-2990.2010.01139.x.

15. *Desai BS, Schneider JA, Li JL, Carvey PM et al.* Evidence of angiogenic vessels in Alzheimer's disease. J Neural Transm 2009;116(5):587-97.

16. *Klohs J, Rudin M, Shims   hek DR, Beckmann N.* Imaging of cerebrovascular pathology in animal models of Alzheimer's disease. Frontiers in aging neuroscience 2014 Mar;13(6):32.

Kristóf Kapitány
Department of Photogrammetry and Geoinformatics, Budapest University of Technology and Economics
H-1111 Budapest, Műegyetem rkp. 3. K building, I/31.
Tel.: (+36) 1 463-1454